MNRAS **429,** 2780–2790 (2013) doi:10.1093/mnras/sts413

Starburst and old stellar populations in the $z \simeq 3.8$ radio galaxies 4C 41.17 and TN J2007−1316

B. Rocca-Volmerange,[1,4⋆] G. Drouart,[1,2] C. De Breuck,[2] J. Vernet,[2] N. Seymour,[3] D. Wylezalek,[2] M. Lehnert,[1] N. Nesvadba[5] and M. Fioc[1]

[1]*Institut d'Astrophysique de Paris, Université Pierre et Marie Curie/CNRS, 98 bis Bd Arago, F-75014 Paris, France*
[2]*European Southern Observatory, Karl-Schwarzschild Strasse, D-85748 Garching bei München, Germany*
[3]*AE (CSIRO Astronomy & Space Science), PO Box 76, Epping, NSW 1710, Australia*
[4]*Université Paris-SUD, F-91405 Orsay Cedex, France*
[5]*Institut d' Astrophysique Spatiale, Bat. 301, F-91405 Orsay Cedex, France*

Accepted 2012 November 14. Received 2012 November 5; in original form 2012 August 10

ABSTRACT

Using the new evolutionary code PÉGASE.3, we undertook an evolutionary spectral synthesis of the optical–IR–submm spectral energy distribution of two distant ($z = 3.8$) radio galaxies, 4C 41.17 and TN J2007−1316. These two radio galaxies were selected from the HeRGÉ (Herschel Radio Galaxies Evolution) Project in particular for their faint active galactic nucleus contribution and because they show evidence of a large stellar contribution to their bolometric luminosity. PÉGASE.3 coherently models the reprocessing of the stellar luminosity to dust emission, allowing us to build UV to IR–submm spectral energy distribution libraries that can then be used to fit spectral energy distributions in the observer's frame. Our principal conclusion is that a single stellar population is insufficient to fit the spectral energy distribution of either radio galaxy. Our best fits are a sum of two evolving stellar populations – a recent starburst plus an old population – plus the thermal emission from an active galactic nucleus (which provides a good fit to the mid-IR emission). The two stellar components are: (i) a massive ($\simeq 10^{11}$ M$_\odot$) starburst $\simeq$30 Myr after formation,which is required simultaneously to fit the far-IR *Herschel* to submm data and the optical data; and (ii) an older massive ($\simeq 10^{11–12}$ M$_\odot$) early-type galaxy population, $\simeq$1.0 Gyr old, which is required principally to fit the mid-IR *Spitzer*/IRAC data. A young population alone is insufficient because an evolved giant star population produces a 1-μm rest-frame peak that is observed in the IRAC photometry. This discovery confirms that many of the stellar populations in high-redshift radio galaxies were formed by massive starbursts in the early Universe. Gas-rich mergers and/or jet–cloud interactions are favoured for triggering the intense star formation necessary to explain the properties of the spectral energy distributions. The discovery of similar characteristics in two distant radio galaxies suggeststhat multiple stellar populations, one old and one young, may be a generic feature of the luminous infrared radio galaxy population.

Key words: galaxies: evolution – galaxies: active – galaxies: stellar content.

1 INTRODUCTION

Large-scale cosmological simulations offer the prospect of constraining theories of galaxy formation and probing the appropriateness of cosmological parameters. However, various problems arise with hydrodynamical and *N*-body simulations when fitting observations. The reason for these difficulties is that there are many physical processes and time-scales that are not well understood, for example the appropriate initial conditions for the models, the detailed structure of dark matter haloes, the time-scale over which mass is accumulated into the halo and onto the galaxy, the details of star formation, the relative roles of major and minor mergers and their importance over cosmic time, the effect of the density of the galactic environment, and the impact of stellar and active galactic nucleus (AGN) feedback. Radio galaxies are known to be massive elliptical types that formed in the early Universe (van Breugel et al. 1998; Pentericci et al. 2001; Zirm, Dickinson & Dey 2003; Lacy

⋆E-mail: rocca@iap.fr

et al. 2011). The puzzling Hubble *K*–*z* diagram, which is bounded on the bright side principally by powerful radio galaxies (Lilly & Longair 1984; De Breuck et al. 2002a) allowed us to identify in the co-moving rest-frame the population of elliptical galaxies, which are young but already massive (10^{12} $M_\odot$), out to high redshifts ($z = 4$; Rocca-Volmerange et al. 2004).

On the other hand, the mid-IR, far-IR and submm emissions from distant radio galaxies have been interpreted as starbursts initiated mainly by major mergers (De Breuck et al. 2010; Ivison et al. 2008, 2012; Engel et al. 2010; Seymour et al. 2010, 2012). These dichotomous results – the old population from the Hubble *K*-*z* diagram and the young population from the need for high rates of star formation in radio galaxies – imply that it is necessary to simultaneously follow the passive evolution of the galaxy as well as that of the ongoing starburst to explain the overall spectral energy distribution (SED). This requires a refined spectrophotometric model, such as our new version of PÉGASE. The code PÉGASE.3 offers the possibility to interpret observations in the observer's frame by using UV-to-submm synthetic libraries built for a wide range of ages. The template SEDs take into account the local $z = 0$ templates corrected for evolution of the stellar population (e-correction) and for redshift (k-correction). In the present paper we tackle a precise, heretofore still debated key issue, namely whether the most distant galaxies, including radio galaxies, are pure starbursts initiated by ongoing mergers or are forming stars continuously on time-scales longer than that generally appropriate for mergers. In radio galaxies, there is also the additional difficulty of the thermal emission from the AGN (perhaps a torus) and scattered light from the AGN, which both contribute to the overall SED, especially in the mid-IR and UV respectively (see Drouart et al. 2012).

We chose two radio galaxies, 4C 41.17 and TN J2007−1316, both at $z = 3.8$, because of their small AGN contribution to the overall SED. We applied the following two selection criteria. (i) There should be a relatively faint scattered light contribution in the rest-frame UV as determined from polarimetric measurements. Polarimetric measurements are the only way to ensure that the continuum is mostly of stellar origin. Indeed, these two galaxies are the only cases for which a clear signature of photospheric absorption lines has been detected (Dey et al. 1997). (ii) There should be a faint contribution of the AGN in the rest-frame 8–12 μm range of the SED. To fit the SED, one and two stellar components are successively tried from an automatic procedure that minimizes the χ^2. We focus on the main properties (type, mass, age and star formation history) of the two stellar populations.

In Section 2, we present the observations of the two radio galaxies for which we have built the continuous optical–IR–submm SEDs after correcting for instrumental effects (differing apertures, flux calibrations, etc.). PÉGASE.3 and the fitting method are described in Section 3. Section 4 presents the best-fitting results of SEDs in the observer's frame, obtained using two evolved stellar populations plus a simple AGN model. Finally, we provide some thoughts on the implications of these results in Section 5, and present our conclusions in the final section. The adopted cosmological parameters are $H_0 = 70\,\mathrm{km\,s^{-1}\,Mpc^{-1}}$, $\Omega_M = 0.3, \Omega_\Lambda = 0.7$.

2 OBSERVATIONS

The two radio galaxies 4C 41.17 ($z \simeq 3.80$) and TN J2007−1316 ($z \simeq 3.84$) are part of a sample of ultra-steep-spectrum (USS) radio sources ($\alpha < -1.3; S_\nu \propto \nu^\alpha$) designed specifically to increase the probability of discovering distant, $z > 3$, radio galaxies (De Breuck et al. 2000). The two targets were specifically selected because of their relatively low level of AGN activity in the rest-frame UV/optical and their strong photospheric and dust signatures, seen respectively in their optical continuum emission and in the cold dust-grain-dominated far-IR emission. The *Spitzer* High Redshift Radio Galaxies (SHzRG) sample, to which these two galaxies also belong, was augmented with *K*-band photometry Seymour et al. (2007, 2008). Most of the complementary optical and submm photometry and data reduction procedures have been described previously (De Breuck et al. 2010). In addition, both galaxies have recently been observed by *Herschel* with the PACS (100- and 160-μm) and SPIRE (250-, 350- and 500-μm) instruments (see also for 4C 41.17, Wylezalek et al. 2012) and are part of the the HeRGÉ (Herschel Radio Galaxy Evolution) Project (Seymour et al. 2012). Optical to submm SEDs, sampling the rest-frame photospheric (UV/optical/near-IR) stellar emission to emission from cold grains (far-IR), are carefully built, paying special attention to aperture effects, flux calibration and flux transmission of the filters used for the observations, and removing the contribution to the fluxes from strong emission lines. For the two galaxies the synchrotron emission is considered as negligible in the wavelength domain analysed, owing to the steep radio spectra of the cores.

2.1 The radio galaxy 4C 41.17

The radio galaxy 4C 41.17 is the archetype of distant radio galaxies ($z = 3.800 \pm 0.003$; Chambers, Miley & van Breugel 1990). A detailed multi-frequency radio analysis with the VLA and MERLIN shows that the radio structure is associated with high-resolution optical imaging *HST* data (see Carilli, Owen & Harris 1994; Miley et al. 1992). The galaxy is detected with a good signal-to-noise ratio and is spatially resolved at the 0.1-arcsec *HST* resolution. Based on both the C III] to C IV line ratio and the strength of the C IV line, Bicknell et al. (2000) suggested that there is an interaction of the high-powered jet with a dense cloud in the halo of 4C 41.17. Such an interaction leads, through high-speed shocks (∼1000 km s^{-1}), to the strong compression of some of the gas, inducing star formation. The bright, spatially extended rest-frame UV continuum emission from this galaxy, aligned with the radio axis, is unpolarized ($P_{2\sigma} < 2.4$ per cent) and shows tell-tale stellar absorption features indicative of ongoing star formation (Dey et al. 1997). Two massive ($M_{\rm dyn} = 6 \times 10^{10}\,M_\odot$) components have been identified from CO (J = 4-3) observations with the IRAM interferometer and interpreted as evidence of mergers (De Breuck et al. 2005). However, the CO (J=1-0) emission line is not detected, and the lower limits obtained are typical of molecular gas in starbursts (Papadopoulos et al. 2005). To complete the broad wavelength coverage of the SED of 4C 41.17, we use the total of the flux from 4C 41.17 within a 6-arcsec field in the K_s-band, which is basically free of strong optical emission lines Graham et al. (1994). For the submm emission we use the results from the JCMT (Dunlop et al. 1994) and IRAM (Chini & Kruegel 1994).

The velocity and dispersion fields were mapped with the integral field spectrograph TIGER/CFHT (Adam et al. 1997) with a 0.61-arcsec spatial sampling. Radial velocities are essentially negative, as the velocity field shows bow shocks with high velocity dispersions. Perpendicular to the main radio axis, a south-west extension of velocity of −600 km s^{-1} and a velocity dispersion of 2000 km s^{-1} are visible. Table 1 contains the photometry data we used to construct the SED of 4C 41.17. The upper limits and data not used by the fitting procedure are also provided for completeness and are also shown in subsequent figures.

Table 1. Photometric data (in red in Figs 3 and 4) of the radio galaxy 4C41.17, including new *Herschel*/SPIRE and PACS observations [α(J2000) = 06^{h}50^{m}52.^{s}098, δ(J2000) = +41°30′30.″53]. Complementary data (lower rows, in green in Figs 3 and 4) are not used for fits, but are provided for completeness.

Filter(λ_c μm)	FWMH	$F_\nu \pm \Delta_\nu$(μJy)	Aperture	Ref.
*HST*_F702W(0.7)	0.15	5.0 ± 0.4	5×5″/2	*a*
KPNO$_I$(0.9)	0.22	4.5 ± 2.6	15″	*b*
NIRC$_J$(1.25)	0.29	5.6 ± 1.1	2″	*c*
NIRC$_{Ks}$(2.15)	0.33	13.6 ± 2.8	8.0″	*j*
IRAC1(3.6)	0.74	23.4 ± 2.4	12″	*d*
IRAC2(4.5)	1.0	27.5 ± 2.8	12″	*d*
IRAC3(5.8)	1.4	35.6 ± 3.7	12″	*d*
IRAC4(8.0)	2.8	36.5 ± 3.5	12″	*d*
PACS(170.)	80	16.2 ± 6. 7 (+3)	Tot	*e*
SPIRE(250.)	100	35.8 ± 3.5 (+3)	Tot	*e*
SPIRE(350.)	150	43.1 ± 3.7 (+3)	Tot	*e*
SPIRE(500.)	200	38.0 ± 4.5 (+3)	Tot	*e*
UKT14(800.)	–	17.4 ± 3.1 (+3)	Tot	*h*
SCUBA(850.)	–	12.1 ± 0. 9 (+3)	Tot	*g*
IRAM(1200.)	–	4.4 ± 0.4 (+3)	Tot	*f*
IRAM(1300.)	–	2.5 ± 0.4 (+3)	Tot	*i*
IRS(16)	–	Upper limit	Tot	*d*
MIPS(24)	6.6	3.7 ±0.4 (+2)	Tot	*d*
PACS(70)	35	Upper limit	Tot	*e*

a: Miley et al. (1992) *f*: Greve et al. (2007)
b: Chambers et al. (1990) *g*: Archibald et al. (2001)
c: van Breugel et al. (1998) *h*: Dunlop et al. (1994)
d: De Breuck et al. (2010) *i*: Chini & Kruegel (1994)
e: This paper, see also Wylezalek et al. (2012)
j: Graham et al. (1994)
Tot: galaxy photometry is totally measured within the instrument aperture.

2.2 The radio galaxy TN J2007−1316, $z = 3.84$

TN J2007−1316 (or WN J2007−1316) is also an USS radio source selected from the 365-MHz TEXAS survey (Douglas et al. 1996) and the NVSS survey (Condon et al. 1998). It was also detected in the 352-MHz WISH survey and is part of the USS sample (De Breuck et al. 2002b). Spectropolarimetry of TN J2007−1316 was obtained with FORS1 on the VLT on three nights from 2002 May 6 to 8 (Fig. 1). For these observations, the 300V grism was used with a 1-arcsec-wide slit oriented north–south and a resolution of ∼10 Å (full width at half-maximum, FWHM). Conditions were photometric, with seeing between 0.5 and 0.9 arcsec. During each night, four equal-length exposures were taken using four different orientations of the half-wave plate (0°, 45°, 22.°5, 67.°5). The total integration time was 27 600 s. The initial data reduction followed standard procedures in the NOAO IRAF package. Because the object is relatively faint in the single 35- or 40-min exposures (each split into o- and e-rays), we needed to pay particular attention to extracting the same physical apertures in each of the individual spectra. We therefore first constructed the total 2D o- and e-ray spectra, and defined 1 × 2.4 arcsec^2 wide apertures from these spectra. We then used the apertures and traces of these spectra to extract the 12 o-ray and 12 e-ray spectra, using the same linear dispersion (2.645 Å pix^{-1}) in order to calculate the polarization in equally sized spectral bins. Finally, we combined these spectra using the median to construct the eight spectra needed to calculate the polarization vector. We followed the procedures of Vernet et al. (2001) to calculate the polarization percentage and position angle. We checked the polarization angle offset between the half-wave plate coordinates and sky coordinates against values obtained for the polarized standard stars

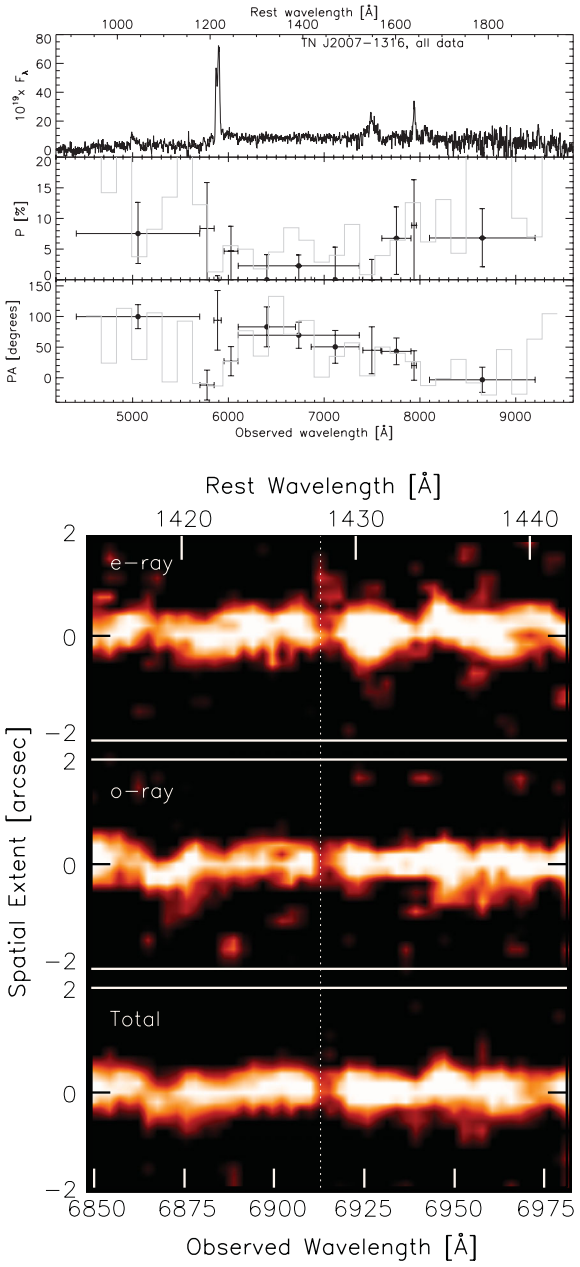

Figure 1. VLT spectropolarimetry of TN J2007−1316. The top panel is divided into three parts: the upper shows the total intensity spectrum, the middle plot is the percentage polarization, and the bottom plot is the polarization angle, as a function of observed wavelength. Continuum bins are denoted by dots. Vertical error bars denote 1σ uncertainties. The grey histograms show the data with a 150-Å binning. The bottom panel is the 2D spectrogram, showing evidence of stellar signatures.

Vela 1 and Hiltner 652: our values are within 1° of the published values, and the polarization percentage is within 0.1 per cent.Table 2 provides the results and data source references.

3 THE EVOLUTIONARY CODE PEGASE.3

The new version of PÉGASE.3 (Fioc, Rocca-Volmerange & Dwek, in preparation) predicts the evolution of the stellar continuum, of the metal and dust content, and the consequent attenuation and re-emission of the UV/optical continuum by dust in a self-consistent manner. With this new version, PÉGASE.3, updated from PÉGASE.2

Table 2. Photometric data of the radio galaxy TN J2007−1316 (in red in Fig. 5), α(J2000) = $20^{h}07^{m}53.^{s}23$, δ(J2000) = $-13°16'43.''6$. Complementary data (bottom lines) are not used for fits, but are given for completeness. The continuum polarization percentage is accurate to within 0.1 per cent.

Filter(λ_c(μm))	FWMH	$F_\nu \pm \Delta_\nu$(μJy)	Aperture	Ref.
R(0.65)	0.06	2.1 ± 0.4	$2.0''^2$	*a*
CFHT$_I$(0.9)	0.22	2.6 ± 0.15	$2.0''^2$	*a*
ISAAC$_H$(1.65)	0.3	9.6 ± 1.0	Tot	*a*
UKIRT$_K$(2.2)	0.3	28.4 ± 1.9	$2.0''^2$	*d*
IRAC1(3.6)	0.74	46.6 ± 4.8	Tot	*a*
IRAC2(4.5)	1.0	52.7 ± 5.7	Tot	*a*
SPIRE(250.)	100.	13.8 ± 6.1 (+3)	Tot	*a*
SPIRE(350.)	150.	16.5± 6.4 (+3)	Tot	*a*
SPIRE(500.)	200.	7.6 ± 3.3 (+3)	Tot	*a*
SCUBA(850.)	–	5.8 ± 1.5(+3)	Tot	*b*
IRAC3(5.8)	1.4	Upper limit	Tot	*a*
IRAC4(8.0)	2.8	135.1 ± 16.9	Tot	*a*
IRS (16.0)	6.0	378.0 ± 113.	Tot	*c*
MIPS1 (24.)	6.6	385.0 ± 40.00	Tot	*c*
PACS(105)	40.	Upper limit	Tot	*a*
PACS(170)	80.	Upper limit	Tot	*a*

a: This paper
b: Reuland et al. (2004)
c: De Breuck et al. (2010)
d: Bornancini et al. (2007)

(www2.iap.fr/pegase; Fioc & Rocca-Volmerange, 1997, 1999b), synthetic SEDs are continuously created from the far-UV to the submm wavelengths at all ages. We built evolutionary scenarios that are consistent with the observed SEDs (and colours) of the full range of Hubble types at $z = 0$. For convenience, we refer to these SEDs by their best fit of morphological Hubble type at $z = 0$, with the understanding that they, by definition, represent the SEDs of galaxies representative of their respective Hubble types in the local Universe.

In PÉGASE.3, the chemical enrichment history is computed in a one-zone model, following the evolution of helium and, most importantly, of metals such as O, Ne, Mg, Si, S, Ca, C, Fe and N. We used the yields from Marigo (2001) for low- and intermediate-mass stars; those of Woosley & Weaver (1995) or Portinari, Chiosi & Bressan (1998) for high-mass stars; and model W7 of Thielemann, Nomoto & Yokoi (1986) for Type Ia supernovae (see details in Fioc et al. in preparation). We assumed that dust formed in circumstellar environments (Dwek 1998): in the stellar winds of asymptotic giant branch (AGB) and Wolf–Rayet stars, only carbon dust is produced if the C/O ratio is larger than 1, and only silicate dust otherwise; in supernovae, as CO is unlikely to form, both carbonaceous and silicate grains may form, but with a lower efficiency than in other sources of dust. To compute the dust emission, we distinguish between two components: star-forming H II regions and the diffuse interstellar medium (ISM). Monte Carlo simulations of radiative transfer are computed, including scattering by dust grains, for geometries typical of discs (exponential profiles for both stars and dust) and elliptical galaxies (King profiles). The path-lengths of photons before escape, absorption, or scattering are obtained from the method of virtual interactions (Városi & Dwek 1999). The attenuation is calculated for a grid of optical depths, albedos and asymmetry parameters, and the value at each wavelength is then interpolated on this grid. For each grain type and size, the probability distribution of temperatures is derived following the procedure detailed in Guhathakurta & Draine (1989); that is, with stochastic heating but assuming the continuous cooling of grains.

To model a medium of higher gas density than the classical ISM we consider that the optical depth depends simultaneously on the column density *NHI* and the current metallicity (see Guiderdoni & Rocca-Volmerange 1987). Following the formalism of Dwek (1998) based on the respective fractions owing to scattering $\kappa_{\rm sca}$ and to extinction $\kappa_{\rm abs}$, the effective optical depth is

$$\tau_{\rm eff} = 1.4\,(\kappa_{\rm abs} + \kappa_{\rm sca})\,K\;\;NHI_{\rm ISM}\,(Z_{\rm C} + Z_{\rm Si})\,m_{\rm H}.$$

In the case of denser absorbing/scattering media, the column density is multiplied by a factor K, where $NHI_{\rm ISM} = 6.8 \times 10^{21}$ atoms cm^{-2} measured by mass units of carbon and silicon in the interstellar medium of our Galaxy.

3.1 PEGASE.3 libraries by galaxy types

Fig. 2 shows an example of the synthetic templates for a S0-type galaxy at various ages as computed by the code PÉGASE.3. Various synthetic libraries of the evolution of SEDs from 0 to 20 Gyr are constructed to simulate the evolution of instantaneous starbursts and of various galaxy types: elliptical (E), lenticular (S0), spiral (Sa, Sb, Sbc, Sc, Sd) and Magellanic irregular (Im) galaxies. Each star formation scenario is defined predominantly by a set of four parameters: star formation law, infall time-scale, epoch of galactic winds for

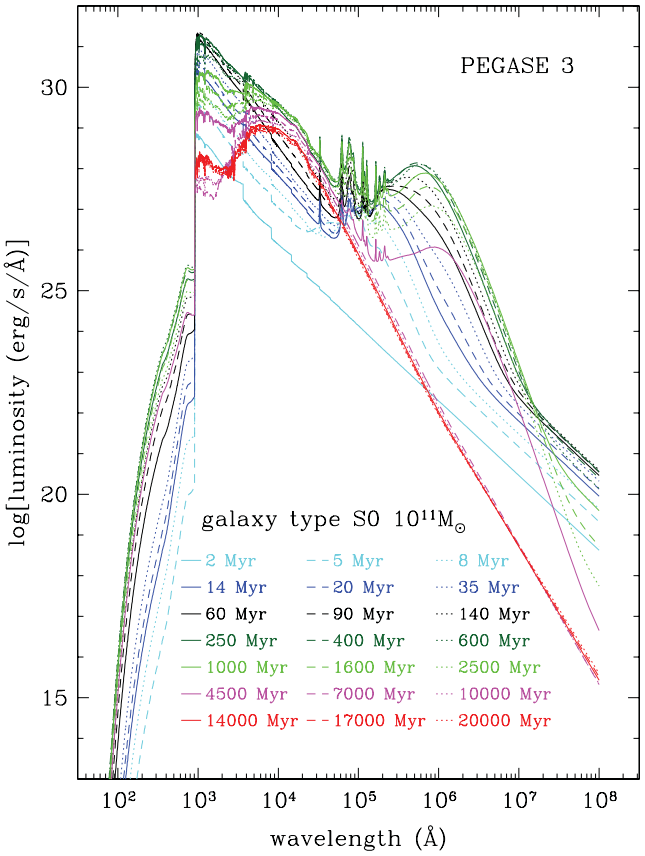

Figure 2. An example of SED templates for a 10^{11} M$_\odot$ S0-type galaxy at various stages of evolution as computed with PÉGASE.3. The 1-μm peak of giant stars appears at ages ≥1 Gyr. Input parameters are: star formation rate = 2×10^{-3} × current gas mass per Myr; an infall time-scale of 100 Myr; galactic winds ejecting gas and dust at 5 Gyr; a Kroupa IMF; and a spheroidal extinction model (see text for details).

early types, and stellar initial mass function (see PÉGASE.2 readme on www.iap.fr/pegase). The parameter set of each type (Table 1; Le Borgne & Rocca-Volmerange 2002; Fioc & Rocca-Volmerange 1997) is chosen to predict $z = 0$ SEDs and colours comparable by type to local observations (Fioc et al. 1997). The robustness of the adopted scenarios is also checked on distant galaxies from the UV to the near-IR Rocca-Volmerange et al. (2004), on faint galaxy surveys analysed by spectral type in the mid-IR (Rocca-Volmerange et al. 2007) and the UV–optical–near-IR (Fioc & Rocca-Volmerange 1999a), and for photometric redshift prediction at high redshift ($z = 4$), which shows good agreement with redshifts obtained spectroscopically (Le Borgne & Rocca-Volmerange 2002).

Instantaneous starbursts are defined such that stars are formed over a period of 1 Myr. Then they passively evolve to the phase at which their far-IR emission is dominated by the circumstellar emission of asymptotic giant branch stars and supernovae (the post-burst phase). The code computes by transfer this IR emission based on the efficiency at which the UV and optical photons are absorbed. In addition to the SEDs according to type, the mass and age of the stellar populations are further outputs from the fitting procedure.

Starburst libraries are computed for a variety of stellar initial mass functions (IMFs). For all scenarios, the IMF was taken as the Kroupa, Tout & Gilmore (1993) IMF, after checking that other classical IMFs did not significantly change our predicted colours and template SEDs. Star formation is initiated at a redshift that we denote as $z_{\rm for}$ (redshift of formation), which we have taken as 10 when cosmic time slowly varies while redshifts increase. While this would imply that the best fits of local SEDs with star formation laws by types correspond to an age of 13 Gyr (adjusted to lower redshift for irregulars, 9 Gyr) for local $z = 0$ galaxies, this should not be taken as the average age of the stellar population, as this is only when the star formation is initiated and not when the bulk of the stellar population forms (this depends on many factors in the the models). Changing $z_{\rm for}$ from $z = 10$ to $z = 20$ or 30 will only vary typical ages of local templates by a small amount ($\leq$0.4 Gyr) and thus result in only inconsequential variations in the SEDs.

3.2 Methodology

An automatic procedure, which uses χ^2 minimization, searches for the best fit of observations with one or the sum of two spectral templates from the set of synthetic libraries (starburst + a variety of SEDs based on best fits of local galaxies with a range of Hubble types). For high-redshift galaxies, we work with template SEDs at redshift z in the observer's frame, by using $z = 0$ SEDs, which fit the SEDs and colours of local galaxies, corrected for cosmological expansion (redshift k-correction) and evolution (age e-correction) using the cosmic time–z relation. For photometry through various filters, apparent magnitudes m^i_λ of galaxy type i, for filter λ, age t and redshift z, are computed by

$$m^i_\lambda(t, z) = M^i_\lambda(t_0, 0) + (m - M)_{\rm bol} + k^i_\lambda(z, t) + e^i_\lambda(z, t)$$

(see Rocca-Volmerange & Guiderdoni 1988 for details), where $M^i_\lambda(t_0, 0)$ is the local absolute magnitude for type i, $(m - M)_{\rm bol}$ is the distance modulus and $k^i_\lambda(z, t)$, and $e^i_\lambda(z, t)$ are the expansion and evolution corrections, computed from PÉGASE.3 synthetic templates.

4 RESULTS OF THE SED FITTING

Because the two z=3.8 radio galaxies are selected for their small AGN contribution to the UV/optical portion of their SEDs, as evidenced by their low level of polarization, simple models of the thermal emission from the AGNs are sufficient for this analysis. The mid-IR SEDs provide an upper limit to the AGN component. We modelled the AGN emission of 4C 41.17 with a blackbody at $T = 600$ K and of TN J2007−1316 with the torus c model of Pier & Krolik (1992) and Krolik & Begelman (1988; see Drouart et al. 2012 for details). A more robust statistical analysis of the contribution of the AGNs in radio galaxies will be conducted for the whole of the HeRGÉ sample. For the two radio galaxies studied here, the range of plausible AGN thermal continuum models has only a minor impact on the results of our stellar SED modelling and will not be discussed further.

4.1 Single-component model fits to the SEDs

Fig. 3 (left) shows the best fits of the observed 4C 41.17 SED with one single burst of star formation with a duration of 1 Myr that is passively evolving for 25 Myr and also a single-component spiral-like evolutionary scenario with an age of 1.6 Gyr. The starburst evolutionary scenario fits the optical and far-IR (*Herschel*) data well but fails to fit the region of the rest-frame 0.4–2 μm (K_s and IRAC/*Spitzer*) SED. The optical peak is due to stellar photospheric emission, and the far-IR/submm peak is due to a fraction of the $N_{\rm Lyc}$ photons absorbed by cold grains within environments of recent star formation. While the starburst episode is consistent with a substantial portion of the SED (see also Seymour et al. 2012, for the infrared data for PKS 1138-262), having to let it evolve for ∼25 Myr suggests that the far-IR peak results from dust produced in and heated by supernovae and AGB stars while the optical (UV-redshifted) emission is due to the photospheres of recently formed massive stars. The AGN component, modelled as a blackbody with a temperature of 600 K, is compatible with the data. The starburst mass, consistent with the best fit of the SED, is $2.7 \times 10^{11}\,{\rm M}_\odot$. In the case of instantaneous starburst, the average stellar metallicity $\langle Z_* \rangle$ corresponds to the gas metallicity when stars were formed (null for a primitive cloud). For low values of $\langle Z_* \rangle$, the far-IR emission is dominated by the self-gas-enrichment of the starburst, measured by the parameter $Z_{\rm C+Si}$ which measure abundances of carbon and silicon. The important point is that from the K_s and IRAC/*Spitzer* photometry, no matter what the exact starburst parameters adopted are, the mid-IR emission is not well fitted.

On the other hand, a model with an older stellar population, such as an early-type spiral Sa scenario with an age of 1.6 Gyr and a stellar mass M_* of $3.7 \times 10^{11}\,{\rm M}_\odot$, fits the optical, near-IR and *Spitzer*/IRAC data rather well but does not fit the far-IR emission (Fig. 3 right). We note, because it is important evidence for the existence of an older population in both radio galaxies, that the SED of an older population shows a peak at ∼1 μm, which is clearly observed. However, despite the obvious advantages to both models in fitting the SED, it is clear that neither single-component model provides even an adequate fit to the overall SED.

4.2 Two-component model fits to the SEDs

Because the one-component fits are inadequate but each individually has features that uniquely fit important regions of the overall SEDs, it seems logical to attempt two-component fits that realize the advantages of each single-component model. To this end, we fit two components, one representing a recent burst of star formation, and the other a passively evolving episode of past star formation (of course constrained by the age of the Universe at $z \sim 3.8$). The best-fit scenario for the radio galaxy 4C 41.17 (Fig. 4) is the sum of

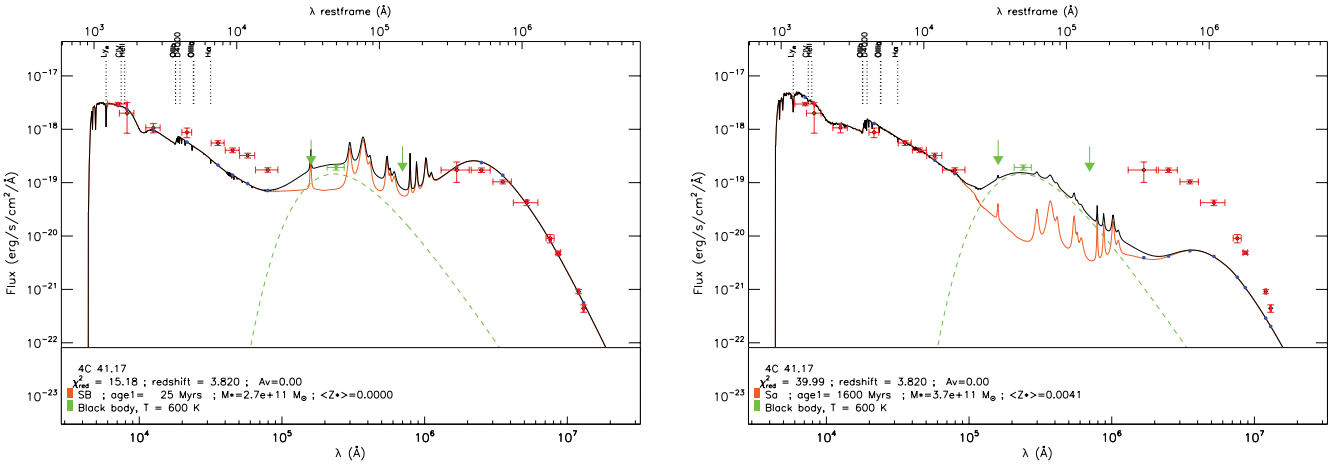

Figure 3. The multi-wavelength SED of 4C 41.17 (dots with red error bars) compared with the sum (black line) of two components: the AGN blackbody at $T_{\rm eff} = 600$ K (dashed green line) plus a stellar component: (left) a starburst at age 25 Myr; (right) a spiral Sa at age (time since $z_{\rm for}$) 1.6 Gyr. The age, stellar metallicity and total stellar mass are derived from the best-fit model. Both of these single-component models are missing a significant fraction of the total energy, either in the near-IR for the starburst or in the far-IR for the Sa-type galaxy evolutionary scenario. Vertical dotted lines mark the position of prominent emission lines. A second component is clearly needed to fit the SED. No intergalactic extinction ($A_V = 0$) is taken into account in the models.

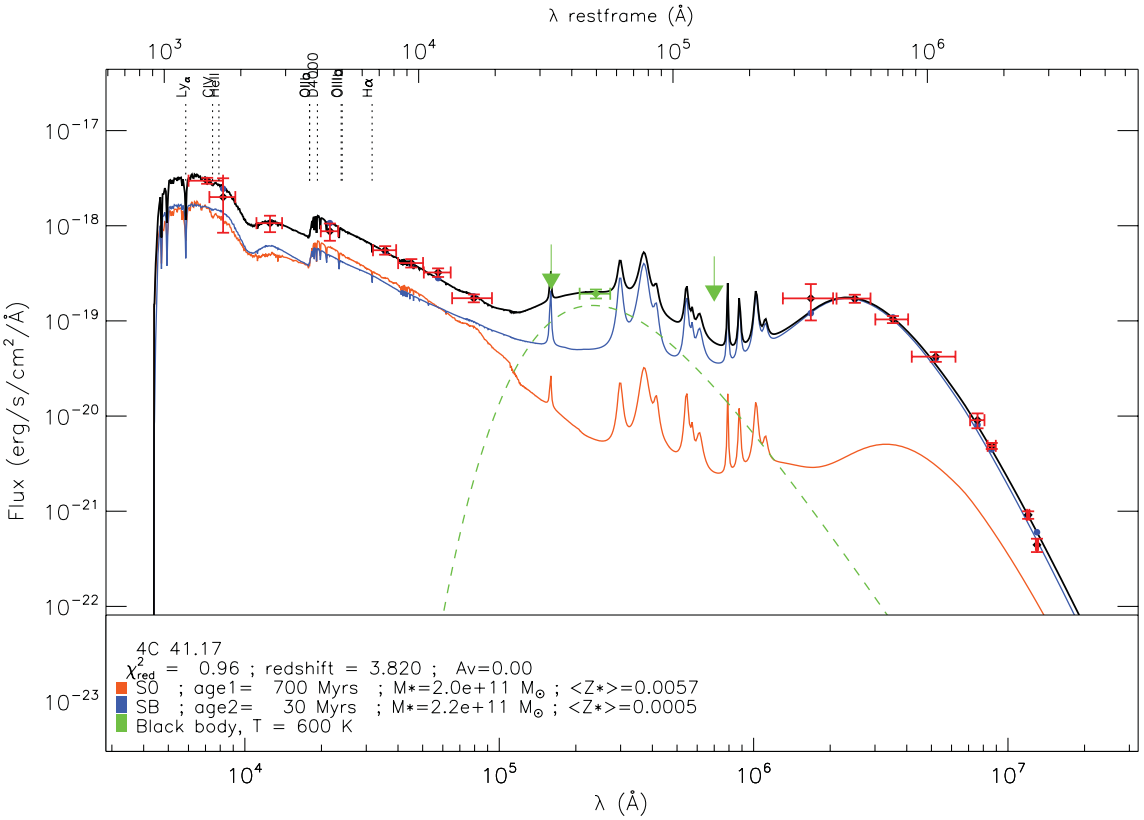

Figure 4. The SED of 4C 41.17 (dots with red error bars) including the new *Herschel* data is best fitted (reduced $\chi^2 = 0.96$) by the sum (black line) of the S0-type population evolutionary scenario at age (time since $z_{\rm for}$) 0.7 Gyr (orange line) and a starburst (SB) 30 Myr after the initial 1-Myr duration burst (blue line) from a dense (10 × standard $\rm NHI_{ISM}$) medium. A $T_{\rm eff} = 600$-K blackbody is used to model the thermal emission from the AGN (green dashed line). Observations not included in stellar fits are displayed in green. As can be seen, by excluding these data, our results are relatively insensitive to the exact model adopted for the thermal emission from the AGN. Vertical dotted lines mark the positions of prominent emission lines. No intergalactic extinction ($A_V = 0$) is taken into account in the models.

two stellar components: a vigorous starburst observed at an age of 30 Myr from a cloud of stellar metallicity $< Z_* > = 5 \times 10^{-4}$ and mass $M_* = 2.2 \times 10^{11}\,{\rm M}_\odot$, and a second population of a massive S0-type scenario with a short e-folding time (see Fig. 2) typical of early-types, observed 0.7 Gyr after its initial formation epoch, with a stellar mass $M_* = 2.0 \times 10^{11}\,{\rm M}_\odot$ and a metallicity $< Z_* > = 5.7 \times 10^{-3}$. Results on stellar components are weakly sensitive to the adopted form of the AGN emission ($T_{\rm eff} = 600$ K blackbody model) in the portions of the SED that are likely to be dominated by the thermal IR emission from the AGN.

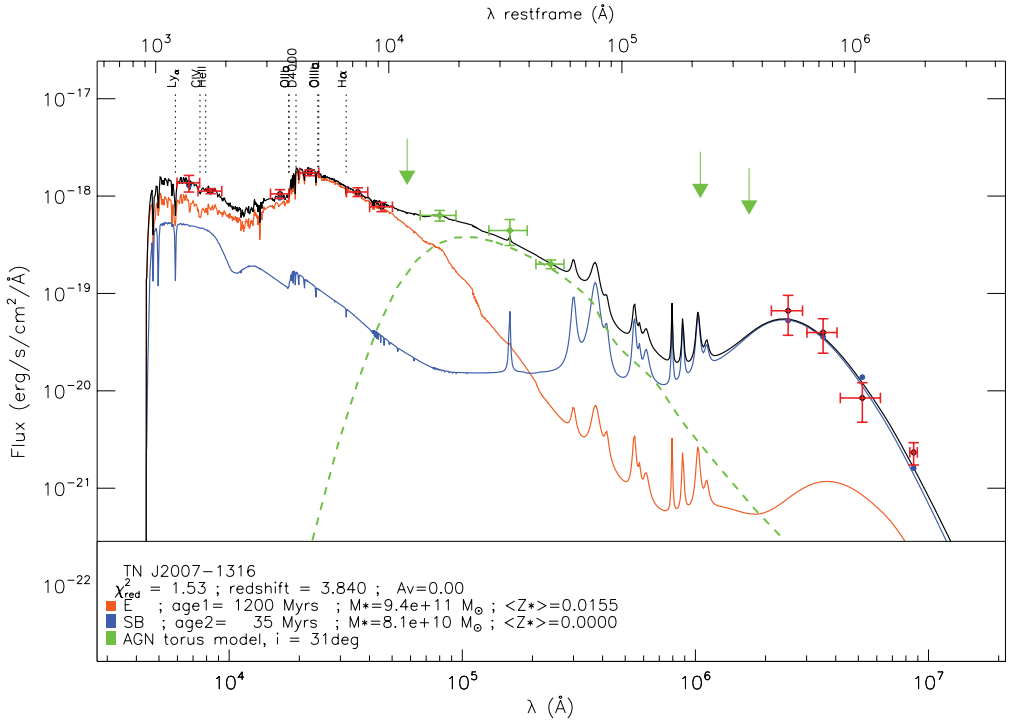

Figure 5. The multi-wavelength SED of TN J2007−1316 (dots with red error bars), including the most recent Herschel data, is fitted (reduced $\chi^2 = 1.53$) by the sum (black line) of an old (1.2-Gyr) elliptical galaxy (orange line) plus a starburst of 35 Myr (blue line) from a dense (10 × standard $\mathrm{NHI_{ISM}}$) medium. The AGN model is the torus c model from Pier & Krolik (1992). Data points shown in green are not included in stellar fits. Vertical dotted lines mark the locations of prominent emission lines in the SED. No intergalactic extinction ($A_V = 0$) is taken into account in the models.

Table 3. Characteristics of the young post-burst at $z = 3.8$: age, stellar mass M_*, initial star formation rate, bolometric luminosity L_{bol}, dust/bolometric luminosity ratio, carbon+silicon $Z_{\mathrm{C+Si}}$ mass fraction, column density factor K (NHI) = $K \times \mathrm{NHI_{ISM}}$, and number of Type II supernovae.

Post-burst	Age (Myr)	M_* (10^{11} $\mathrm{M_\odot}$)	$\mathrm{SFR_{init}}$ (10^5 $\mathrm{M_\odot}$ $\mathrm{yr^{-1}}$)	L_{bol} (10^{46} erg $\mathrm{s^{-1}}$)	$L_{\mathrm{dust}}/L_{\mathrm{bol}}$	$Z_{\mathrm{C+Si}}$	K (NHI)	n_{SNII} (10^7 $\mathrm{Myr^{-1}}$)
in 4C 41.17	30	2.2	2.6	8.0	0.96	0.026	10	7.1
in TN J2007−1316	35	0.8	0.1	0.3	0.97	0.025	10	0.3

The results on the stellar components derived from the best fit for TN J2007−1316 (Fig. 5) are generally similar to those for 4C 41.17, namely there is the need for a young starburst and an older stellar population similar to that of a local massive galaxy evolved by a redshift of 3.8. Specifically, the fit requires a starburst of very low metallicity evolved for 35 Myr with a total stellar mass of $M_* = 8.1 \times 10^{10}$ $\mathrm{M_\odot}$ and a second component consistent with that of an evolved massive early-type galaxy observed at an age of 1.2 Gyr (after z_{for}) with an average stellar metallicity ($< Z_* > = 1.5 \times 10^{-2}$) and a significant stellar mass ($M_* = 9.4 \times 10^{11}$ $\mathrm{M_\odot}$).

4.2.1 A massive post-burst in distant radio galaxies

For the two $z = 3.8$ radio galaxies, the fact that they fit simultaneously the optical ($\simeq 1500$ Å rest-frame) and crucially the far-IR SED provided by the *Herschel*/submm data suggests that both galaxies underwent a massive starburst several tens of Myr ago (a post-burst). The modelling of the far-IR emission depends on the metal enrichment of carbon and silicon, $Z_{\mathrm{C+Si}}$, while the observed UV–optical emission is dependent on the amount of absorbed photospheric emission intrinsic to the young stellar population. The main characteristics of the fitted young post-burst scenario are summarized in Table 3. The best fit is a result of having to balance the far-IR and optical luminosities and spectral shapes, measured by the reduced χ^2_{red} minimum. A younger age increases the number of Lyman continuum photons but decreases the metal-enrichment, favouring the direct photospheric emission relative to dust emission. Older ages have the opposite effect. Because of this dependence, the starburst mass and age are well constrained and unique. All other parameters of Table 3 ($Z_{\mathrm{C+Si}}$ metallicity, supernova number, high density value) are not free parameters, but are derived from chemical evolution. We recall that the mean metallicity of stars $\langle Z_* \rangle$, as indicated in the legends, only traces the gas metallicity when stars were formed. In the case of starbursts, this parameter is the initial gas metallicity and remains constant with age while gas metallicity evolves and is, largely dominated at an age of 30 Myr by the intrinsic gas enrichment arising from the passive evolution of the starburst scenario.

For the radio galaxy 4C 41.17 (Fig. 4 and Table 3) the new *Herschel*/submm observations are well modelled by the cold-grain emission of the highly massive and metal-enriched ($Z_{\mathrm{C+Si}} = 0.026$) stellar environments. This post-burst population was triggered

30 Myr earlier in a starburst with a duration of 1 Myr (instantaneous) and a star formation rate of 2.6×10^5 $M_\odot$ yr^{-1} (current stellar mass corrected for already dead stars at an age of 30 Myr). The rapid evolution of the most massive stars (a few 10^7 yr) means that they have already evolved to supernovae and AGB stars when the post-burst is observed, enriching the interstellar medium. This implies that supernova explosions ($n_{\rm SNII} = 7.1 \times 10^7$ by Myr) and AGB stars with circumstellar envelopes are dominant. A dense medium with high column density (a factor $K = 10 \times$ the column density measured in the Galactic ISM, $\rm NHI_{ISM}$) is required by the far-IR data, implying 10^{22-23} atoms cm^{-2}. Such column densities have been found in radio galaxies (Mullaney et al. 2010). This post-burst in the far-IR dominates the total luminosity (96 per cent). In the radio galaxy TN J2007−1316 (Fig. 5 and Table 3), the starburst age is 35 Myr with a mass of 8.1×10^{10} $M_\odot$ and an initial metallicity of zero, probably a primitive cloud. This suggests that most of the necessary metal enrichment to explain the far-IR emission ($Z_{\rm C+Si} = 0.025$) is attributable to self-enrichment of the young stellar population.

4.2.2 *The importance of the 1-μm peak*

Figs 4 and 5 show the typical energy distribution of an old stellar population in the *K* band and through *Spitzer*/IRAC filters (from the 4000-Å discontinuity to the typical 1-μm peak in the rest-frame). The evolution of early-type galaxies is characterized by a short ($\simeq$1 Gyr) intense star formation episode. This old population is seen in both targets, perhaps suggesting that it is a generic feature of radio galaxies. For both radio galaxies, this component has an age that is a significant fraction of the Hubble time at $z = 3.8$. We recall that we have characterized the ages as the time from the formation redshift $z_{\rm for}$, which for 4C 41.17 and TN J2007−1316 is roughly 0.7 and 1.2 Gyr, respectively. However, acceptable fits allow for a range of age of at least a factor of 2 around these nominal values. We also note that the bulk of the stars in this old population formed more recently than the times listed. This peak in the SED arising from evolved giant stars only evolves slowly and has been identified at all redshifts. This result supports our analysis of the Hubble *K*-band diagram (Rocca-Volmerange et al. 2004), predicting already massive and old galaxies at $z \geq 4$. Table 4 presents the characteristics of the evolved old component. Stellar masses are 2×10^{11} $M_\odot$ for 4C 41.17 and $\sim 10^{12}$ $M_\odot$ for TN J2007−1316. These masses are higher than that of the young starburst mass and perhaps suggest previous episodes of merging at earlier epochs, compatible with some galaxy formation models (Lackner et al. 2012). The contribution of the AGN to MIPS/*Spitzer* data, modelled by a simple blackbody law at $T_{\rm eff} = 600$ K as shown in Fig. 4 (dashed green line), and by a more sophisticated torus c-model (adapted from Pier & Krolik 1992, by G. Drouart) for the radio galaxy TN J2007−1316 (Fig. 5, dashed green line), does not change our conclusions: for these two radio galaxies, the AGN emission is not significant in the near-IR domain at $z = 3.8$.

5 DISCUSSION

The SEDs of the $z = 3.8$ radio galaxies 4C 41.17 and TN J2007−1316 are analysed with two stellar (young and old) components and an AGN model. The evolutionary spectral synthesis used to fit the data is based on a variety of template libraries, including instantaneous starbursts and evolutionary scenarios designed to fit the SEDs of local Hubble-type galaxies. Each scenario is characterized by a star formation time-scale: ∼1 Myr for the instantaneous starburst, and ∼1 Gyr for ellipticals to ∼10 Gyr for spirals (see Rocca-Volmerange et al. 2004). In the case of gas-dependent star formation laws, star formation time-scales are regulated by the accretion and galaxy-scale outflows of gas. One template library is built for each scenario. For starbursts, various standard IMFs are modelled in these template libraries. Because in evolutionary models such as PÉGASE.3 IMFs are all normalized to 1 $M_\odot$ and held fixed throughout the evolution, changing the IMF does have an effect on the relative rate of metal-enrichment and the dust fraction, but has only a minor effect on the best-fit results of the SED. Although only weakly constrained, all of our best fits favour a Kroupa et al. (1993) IMF. The most robust determinations from our fitting analysis are the relative ages and total stellar mass of each best-fit scenario. For the two galaxies, our results suggest that the shape of the SEDs arises from a vigorous recent starburst superimposed on a relatively evolved population whose formation was initiated at early epochs ($z_{\rm for} \geq 10$; but this is not when the bulk of the stellar population was formed, only when the star formation was initiated within the context of the scenarios used to model the SEDs). For the young starburst component, our results suggest an age of ∼30 Myr with a stellar mass of $\simeq 10^{11}$ $M_\odot$. The two peaks seen respectively in the optical and in the far-IR/*Herschel* are the data that constrain this fitted component the most. This is because of the time-scale for dust production in the post-burst AGB and SN populations. Of much lower precision is the age of the older component, which is mainly constrained by the peak in the rest-frame at 1 μm owing to slowly evolving giant stars. This slow evolution means that a wide variety of ages could in principle fit the data roughly equally well, but all best-fit models suggest relatively old ages (hundreds of Myr). The best fits are that of an S0 galaxy with an age of 700 Myr for 4C 41.17 and an elliptical galaxy scenario with an age of 1200 Myr for TNJ 2007−1316. Both are early-types with a ∼1-Gyr time-scale and masses of $\simeq 10^{11-12}$ $M_\odot$. To check the sensitivity of the 4C 41.17 results to ages of models, we tested the relative variations in χ^2 for different models. We maintain an instantaneous starburst as the first component. Replacing the second component by another starburst of 1 Myr duration induces a χ^2 variation of 10 per cent and an age reduction of 80 per cent with deeper Balmer lines. Replacing the second component by a later-type (Sa) scenario with a star formation scale of a few Gyrs induces a χ^2 variation of 5 per cent and an age increase of 120 per cent.

For TN J2007–1316, no scenario other than that of ellipticals is acceptable within a χ^2 variation of 400 per cent. We also tested (Fig. 6) a second component of an early-type model experiencing

Table 4. Characteristics of the old-star population at $z = 3.8$: age, stellar mass M_*, current star formation rate, bolometric luminosity, dust/bolometric luminosity ratio, carbon+silicon dust mass fraction, numbers of Type Ia and Type II supernovae.

Early-type	Age (Gyr)	M_* (10^{11} $M_\odot$)	$\rm SFR_{current}$ ($M_\odot$ yr^{-1})	$L_{\rm bol}$ (10^{45} ergs s^{-1})	$L_{\rm dust}/L_{\rm bol}$	$Z_{\rm C+Si}$	$n_{\rm SNIa}$ (10^5 Myr^{-1})	$n_{\rm SNII}$ (10^5 Myr^{-1})
4C 41.17	0.7	2.0	243	8.2	0.522	0.026	0.8	19.2
TN J2007 − 1316	1.2	9.4	77	10.0	0.096	0.023	3.8	6.7

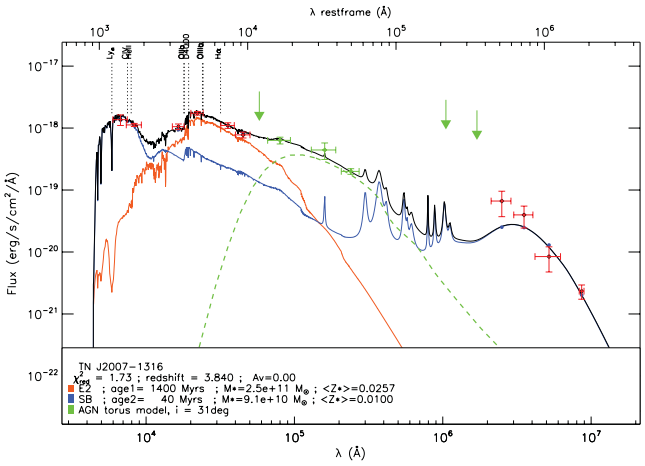

Figure 6. Best fit (reduced $\chi^2 = 0.98$) of the multi-wavelength SED of TN J2007−1316 (dots with red error bars) with the sum (black line) of a 18-Myr starburst (blue line) plus an early-type galaxy (1.4 Gyr) after an episode of galactic winds (orange line) (by ejecting gas and dust, they stop any further star formation). Masses and ages vary by ≤50 per cent compared with the results of Fig. 5.

galactic winds at early epochs (at an age of 1 Gyr). The 1-μm peak is then better fitted to IRAC data at an age of 1.4 Gyr and summed with a younger (40-Gyr) starburst. For the two populations, ages do not vary by more than 50 per cent.

In summary for these two powerful radio galaxies, a young post-burst and an evolved component with a short time-scale (∼1 Gyr) are the best solutions. The time-scale for both the increase in the metallicity with time and the relative fraction of dust in the ISM that produced the far-IR emission are calculated in a self-consistent manner based on stellar yields and the production of dust by stars. The relatively poor time resolution in fitting the broad-band continuum with stellar synthesis models for high-redshift galaxies does not allow us to discuss anything but simple evolutionary models (not, for example, successive short bursts, which would look more like continuous star formation in the models). Long star formation time-scales result in two cumulative effects: increasing metal and dust fractions, and a simultaneous decrease in the photospheric emission of massive stars. Because of these effects, the parameter range that simultaneously fits both the rest-frame optical and infrared portion of the SEDs is relatively narrow. That is why it is important to perform this analysis on multiple sources: if they give consistent results, this means that the general characteristics of the best fits are likely to be robust.

The general conclusions we can make are that the masses are probably in the range $10^{10–11}$ $M_\odot$ for recent starbursts and $10^{11–12}$ $M_\odot$ for the early-type evolutionary scenarios used to fit the data. Starbursts and evolved galaxies have mass ratios of 1:1 to 1:10 typical of major mergers, so that any mass interchange will not significantly affect results. Moreover, all mergers are gas-rich, inducing an efficient star formation.

5.1 Star formation in 4C41.17

What is triggering such intense star formation in distant radio galaxies? One of the most striking features of these distant SEDs is the double peak of starburst activity, in the far-IR *Herschel* from dust, and in the optical from star photospheres. The instantaneous starburst model evolves to an age of ∼30 Myr, probably dominated by supernovae and AGB stars. The huge stellar mass, ≃2.2 10^{11} $M_\odot$, corresponds to a rapid metal-enrichment from a non-primitive cloud ($Z_* = 5 \times 10^{-4}$). The emission is issued from a gas of high density, characterized by the factor $K = 10$, describing an ISM 10 times denser than the classical ISM.

Table 5. Starburst/old population ratios.

Radio galaxy	Age	Stellar mass	SNII number	K
4C 41.17	30:700	2.2:2.0	71:1.9	10:1
TNJ 2007 − 1316	35:1200	8:94	30:6.7	10:1

A model has already been proposed for 4C 41.17, a template of the so-called alignment effect (Chambers et al. 1990; Miley et al. 1992). Based on the jet–cloud interaction inducing star formation by shocks, suggested by many authors from 1980 onwards, it was revisited by Bicknell et al. (2000) in the light of *HST* and radio emission-line data (Dey et al. 1997; van Breugel et al. 1998). The authors agree on a set of parameters: a baryonic mass of ∼8× 10^{10} $M_\odot$, a star formation time-scale of a few Myr, a dynamic radio galaxy age of ∼30 Myr, and a high density of ∼1–10 cm^{-3}. All these values are compatible with our stellar population model, favouring the jet–cloud interaction model for triggering star formation at high redshifts. Another favourable argument for this scenario, at a much lower rate, is the star formation by jet–cloud interaction discovered in the core of NGC 1068 with the high angular resolution of NaCo/VLT (Exposito et al. 2011).

The dense medium measured by a column density factor $K = 10$, meaning 10^{22-23} atoms cm^{-2}, only seen in the starburst component requires justification. A better spatial resolution associated with a more refined 3D spectroscopy with the new generation of instruments (MUSE/VLT) will solve the location of star formation activity and the feedback measurement.

The coincidence of the short time-scales of both starburst and jet interaction implies a similar causal origin. In that case, the post-burst we are seeing at work is only an episode of an active merger process. Many other arguments would favour massive gas-rich mergers at high redshifts. The discovery of huge CO components (De Breuck et al. 2005; Engel et al. 2010; Ivison et al. 2010) provide evidence of major mergers in powerful distant radio galaxies. Another convincing remark in favour of gas-rich mergers is that to form such huge stellar masses in short episodes requires large volumes of gas at high densities, significantly larger than the narrow volumes concerned by the jet-cloud interaction. Table 5 gives the characteristics of the intervening masses, with mass ratios typical of major mergers of young and old components of various metallicity, occasionally of primitive gas, implying the existence of several star generations through merger processes.

5.2 The old early-type stellar population

Local early-type galaxies are generally not luminous in the far-IR (Xilouris et al. 2004), which has been interpreted to be the result of galactic winds driven by the evolved populations (Type I supernovae; Mathews & Baker 1971). The other possible mechanism for driving winds is the mechanical and radiative energy from intense starbursts. For example, in the local archetypal starburst galaxy M82, galactic winds were recently studied with *Herschel*/PACS by (Contursi et al. 2012). The authors propose that cold clouds are entrained in the galaxy disc outflow. At high redshifts, star formation activity is intense enough at the earliest epochs to induce intense winds, which may also entrain the molecular and neutral atomic

hydrogen, driving it out of the galaxy. This assumption will possibly be statistically analysed on the entire HeRGÉ sample.

The new important result is the emergence in the mid-IR (optical rest-frame) of an (already evolved) stellar component, which is seen through a specific window (IRAC filters). The age and huge stellar mass of this old population is calibrated on the SEDs of two selected radio galaxies, in particular when galactic winds are imposed. At an age of ∼1 Gyr, the evolved stellar population is giant stars, creating the well-known peak at 1 μm (rest-frame; Fig. 2). All these results favour the presence of very massive early-type galaxies initiated at early epochs $z_{for} > 10$, which must have grown very rapidly. Because of the insufficient time resolution, the declining continuous star formation laws, as used in PÉGASE.3 and other codes, could also be considered as a series of successive starbursts with intensities declining with time. From this point of view, which is also consistent with the data, the hierarchical assembly history of the most massive ($\sim 8 \times 10^{12}$ M$_\odot$) haloes in a ∼3-Gpc^3 volume as proposed in Li et al. (2007) to form populations of $z = 6$ quasars would be compatible with our results.

5.3 The link with radio-quiet massive galaxies

The discovery of these $z = 3.8$ old stellar components in powerful radio galaxies with a superposed starburst in a high-density medium warrants a comparison with radio-quiet early-type high-z galaxies. These radio quiet galaxies have median stellar masses of $\sim 4 \times 10^{11}$ M at $z = 2.0$–2.7 (Kriek et al. 2006). Their mass estimates are probably underestimated, because observations were through the Gemini Ks filter, likely missing the dominant *K*-band stellar population redshifted in the Spitzer filters. However, the comparison with powerful radio galaxies is justified because their respective masses are of the same order. Moreover, deep and high-resolution images obtained with *HST*/NICMOS and /NIC2 and Keck (van Dokkum et al. 2008; Stockton et al. 2008) are associated with the presence of massive discs of old stars at high redshifts with remarkably small sizes (a median effective radius $r_{\rm eff} = 0.9$ kpc). Cosmological surface brightness dimming has a strong impact on the perceived morphology of distant galaxies and probably explains generally why discs are basically undetectable at $z \geq 1.5$. The decrement due to dimming is of ∼7 mag at redshift 3.8. Only the central disc and spheroidal components are of sufficiently high surface brightness to be detectable, even in deep images (Stockton et al. 2008).

If radio-load galaxies are a subpopulation of the massive radio-quiet galaxies that are undergoing an episode of vigorous star formation, it may well be that the powerful AGNs illuminate the surrounding gas and dust in the disc over larger scales than would not otherwise be visible on account of surface brightness dimming. Even the continuum emission would be affected owing to the scattering of the AGN continuum by dust. Moreover, in the population of radio-quiet massive galaxies, the stellar population does not have the massive young stellar component we have observed in IR-luminous powerful radio galaxies, and therefore would be less luminous in both the far-IR and in the optical, perhaps below the threshold of detectability. The massive evolved starburst in IR-luminous powerful radio galaxies contributes to the illumination of the disc over larger scales, giving values above the surface brightness threshold. Observing extended emission preferentially in radio galaxies confirms the coexistence of the radio and starburst activity in the short star-forming episode perhaps initiated by gas-rich mergers. Of course, the jet would also have an impact through its interaction with the surrounding gas, namely by compressing and heating it. This shaping of the gas by the radio jet may also lead to stronger extended emission in both the emission lines and the continuum.

More knowledge on the kinematics and apparent morphology, which is strongly modified by distance effects, is also required for justifying the spheroidal structure of early-type galaxies. In the case of radio galaxies, all these properties have to be associated with the presence of a supermassive black hole. Future studies will focus on the luminosity relationship between AGNs and star formation activity of a larger sample of HeRGÉ galaxies.

6 CONCLUSIONS

From the PÉGASE.3 evolutionary spectral synthesis of two $z = 3.8$ radio galaxies, the SED fitting over a large wavelength range (UV/optical to far-IR/submm) identifies two distinct stellar components. The originality and specificity of the analysis is to work in the observer's frame by using robust local templates, corrected at high z for the expansion of the Universe (k-corrected) and for evolution owing to distance (e-corrected), following scenario libraries by types of the code PÉGASE.3. At any time, synthetic templates are continuously computed with coherent UV/optical stellar emission and dust absorption re-emitted in the far-IR. Instantaneous (1 Myr) starbursts and a variety of scenarios of the Hubble sequence, varying with star formation time-scales over 1–10 Gyr, are considered for building template libraries. Best SED fits are derived in the observer's frame by a χ^2 algorithmic procedure on a model incorporating two stellar components, plus a simple AGN model.

The main results are similar for the two galaxies at $z = 3.8$, as follows.

(i) One single component is unable to explain the complete SED, whatever types and ages are considered.

(ii) The sum of two stellar components gives the best SED fits, as detailed in the following points:

(a) A 1-Myr starburst, observed at an age of 30 Myr, forming a huge stellar mass ∼10^{11} M$_\odot$ in a dense (10 × standard ISM) medium, dominant in the far-IR *Herschel* to submm and in the optical domains.

(b) The discovery in the *K* band to *Spitzer*/mid-IR domains (1 μm rest-frame) of an already evolved (∼1 Gyr at $z = 4$) population.

(iii) The evolved stellar component is compatible with an early-type galaxy (S0-elliptical) initiated at early epochs ($z_{for} \geq 10$), with possible galactic winds.

(iv) The mass of the evolved component is huge, 10^{11-12}M$_\odot$ for the two galaxies at $z \simeq 4$.

(v) The possibility of a gas-rich merger (associated with a possible jet–cloud interaction) is favoured.

Over the longer term, we intend to include a more refined modelling of the AGN contribution to the overall SED in the PÉGASE.3 evolutionary synthesis models and to model the optical, *Herschel*/submm and *Spitzer* SED data of the HeRGÉ sample over its entire redshift range ($1 \leq z \leq 5$).

ACKNOWLEDGMENTS

This work was based on observations taken with the European Southern Observatory Very Large Telescope, Paranal, Chile, with program ID 069.B-0078. It is also based in part on observations made with Herschel, a European Space Agency Cornerstone Mission with significant participation by NASA.

We finally thank the referee Dr Alan Stockton for his helpful comments and suggestions, which aided us in clarifying our arguments.

REFERENCES

Adam G., Rocca-Volmerange B., Gerard S., Ferruit P., Bacon R., 1997, A&A, 326, 501
Archibald E., Dunlop J., Hughes D., Rawlings S., Eales S., Ivison R., 2001, MNRAS, 323, 417
Bicknell G. V., Sutherland R. S., van Breugel W. J. M., Dopita M. A., Dey A., Miley G. K., 2000, ApJ, 540, 678
Bornancini C. G., De Breuck C., de Vries W., Croft S., van Breugel W., Röttgering H., Minniti D., 2007, MNRAS, 378, 551
Carilli C. L., Owen F. N., Harris D. E., 1994, AJ, 107, 480
Chambers K. C., Miley G., van Breugel W. J., 1990, ApJ, 363, 21
Chini R., Kruegel E., 1994, A&A, 288, L33
Condon J. et al., 1998, AJ, 115, 1693
Contursi A. et al., 2012, arXiv:1210.3496
De Breuck C., van Breugel W., Röttgering H., Miley G., 2000, A&A, 143, 303
De Breuck C., van Breugel W., Stanford S. A., Röttgering H., Miley G., Stern D., 2002a, AJ, 123, 637
De Breuck C., Tang Y., de Bruyn A. G., Röttgering H., van Breugel W., 2002b, A&A, 394, 59
De Breuck C., Downes D., Neri R., van Breugel W., Reuland M., Omont A., Ivison R., 2005, A&A, 430, L1
De Breuck C. et al., 2010, ApJ, 725, 36
Dey A., van Breugel W., Vacca W., Antonucci R., 1997, ApJ, 490, 698
Douglas J. N., Bash F. N., Bozyan F. A., Torrence G. W., Wolfe C., 1996, AJ, 111, 1945
Drouart G., De Breuck C., Vernet J., Laing R. A., Seymour N. et al., 2012, A&A, 548, 45
Dunlop J. S., Hughes D. H., Rawlings S., Eales S. A., Ward M. J., 1994, Nat, 370, 347
Dwek E., 1998, ApJ, 501, 643
Engel H. et al., 2010, ApJ, 724, 233
Exposito J., Gratadour D., Clénet Y., Rouan D., 2011, A&A, 533, 63
Fioc M., Rocca-Volmerange B., 1997, A&A, 326, 950
Fioc M., Rocca-Volmerange B., 1999a, A&A, 344, 393
Fioc M., Rocca-Volmerange B., 1999b, arXiv:astro-ph/9912179
Graham J. R. et al., 1994, ApJ, 420, L5
Greve T. R., Stern D., Ivison R. J., De Breuck C., Kovács A. M, Bertoldi F., 2007, MNRAS, 382, 48
Guhathakurta P., Draine B. T., 1989, ApJ, 345, 230
Guiderdoni B., Rocca-Volmerange B., 1987, A&A, 186, 1
Ivison R. J. et al., 2008, Cat. 83800199
Ivison R. et al., 2010, A&A, 518, L31 (arXiv:1206.4046)
Kriek M. et al., 2006, ApJ, 645, 44
Krolik J. H., Begelman M. C., 1988, ApJ, 329, 702
Kroupa P., Tout C. A., Gilmore G., 1993, MNRAS, 262, 545
Lackner C. N., Cen R., Ostriker J. P., Joung M. R., 2012, MNRAS, 425, 641
Lacy M., Petric A. O., MartÃnez-Sansigre A., Ridgway S. E., Sajina A., Urrutia T., Farrah D., 2011, AJ, 142, 196
Le Borgne D., Rocca-Volmerange B., 2002, A&A, 386, 446
Li Y. et al., 2007, ApJ, 665, 187
Lilly S. J., Longair M. S., 1984, MNRAS, 211, 833
Marigo P., 2001, A&A, 370, 194
Mathews W. G., Baker J. C., 1971, ApJ, 170, 241
Miley G. K., Chambers K. C., van Breugel W. J. M., Macchetto F., 1992, ApJ, 401, 69
Mullaney J. R., Alexander D. M., Huynh M., Goulding A. D., Frayer D., 2010, MNRAS, 401, 995
Papadopoulos P., Greve T. R., Ivison R. J., De Breuck C., 2005, A&A, 444, 813
Pentericci L., McCarthy P. J., Röttgering H. J. A., Miley G. K., van Breugel W. J. M., Fosbury R., 2001, ApJS, 135, 63
Pier E. A., Krolik J. H., 1992, ApJ, 401, 99
Portinari L., Chiosi C., Bressan A., 1998, A&A, 334, 505
Reuland M., Röttgering H. J. A., van Breugel W., De Breuck C., 2004, MNRAS, 353, 377
Rocca-Volmerange B., Guiderdoni B., 1988, A&AS, 75, 93
Rocca-Volmerange B., Le Borgne D., De Breuck C., Fioc M., Moy E., 2004, A&A, 415, 931
Rocca-Volmerange B., de Lapparent V., Seymour N., Fioc M., 2007, A&A, 475, 801
Seymour N. et al., 2007, ApJS, 171, 353
Seymour N. et al., 2008, ApJ, 681, L1
Seymour N., Symeonidis M., Page M. the HerMES consortium, 2010, arXiv:1012.5085
Seymour N. et al., 2012, ApJ, 755, 146
Stockton A., McGrath E., Canalizo G., Iye M., Maihara T., 2008, ApJ, 672, 146
Thielemann F.-K., Nomoto K., Yokoi K., 1986, A&A, 158, 17
van Breugel W. J. M., Stanford S. A., Spinrad H., Stern D., Graham J. R., 1998, ApJ, 502, 614
van Dokkum P. G. et al., 2008, ApJ, 677, L5
Városi F., Dwek E., 1999, ApJ, 523, 265
Vernet J., Fosbury R. A. E., Villar-Martín M., Cohen M. H., Cimatti A., di Serego Alighieri S., Goodrich R. W., 2001, A&A, 366, 7
Woosley S. E., Weaver T. A., 1995, ApJS, 101, 181
Wylezalek D. et al., 2012, MNRAS, in press (arXiv:1210.6361)
Xilouris E. M., Madden S. C., Galliano F., Vigroux L., Sauvage M., 2004, A&A, 416, 41
Zirm A. W., Dickinson M., Dey A., 2003, ApJ, 585, 90

This paper has been typeset from a TEX/LATEX file prepared by the author.